Study of a binder based on alkaline activated limestone

Annelise Cousture, Norbert Renault, Jean-Louis Gallias, Khadim Ndiaye

Study of a binder based on alkaline activated limestone

Annelise Cousture[a], Norbert Renault[a], Jean-Louis Gallias[a], Khadim Ndiaye[a]

[a] CY Cergy Paris Université, L2MGC, F-95000 Cergy, France

annelise.cousture@cyu.fr, norbert.renault@cyu.fr, jean-louis.gallias@cyu.fr, khadim.ndiaye@cyu.fr

Corresponding author: Annelise COUSTURE, annelise.cousture@cyu.fr

Abstract: Binders based on the alkaline activation of raw materials is a subject of increasing importance for construction. This study focuses on a new non-hydraulic binder based on the alkali-activation of limestone by an aqueous solution of sodium hydroxide. An optimized mortar of about 20 MPa compressive strength, made with siliceous sand, was studied by XRD, FTIR and SEM-EDX analyses showing that crystalline pirssonite and portlandite are the reaction products responsible of the cohesive capacity of the binder. A methodology based on thermal gravimetric analysis was applied to quantify the products formed and the consumption of reagents with high reliability.

Keywords: alkali-activation, limestone, pirssonite, portlandite, thermal analysis

Abbreviations: AS/L: Alkaline Solution to limestone ratio; DTA: Differential Thermal Analysis; EDX: Energy-Dispersive X-ray spectroscopy; FTIR: Fourier Transform Infrared spectroscopy; SEM: Scanning Electron Microscope; S/L: Sand to Limestone ratio; TGA: Thermogravimetric Analysis; W/B: water to binder ratio; XRD: X-Ray Diffraction.

1. Introduction

During at least the last 20 years the study of alkaline activation has grown exponentially, even though research in this field began in the 1940s [1]. In the absence of clinker, blast furnace slag was activated by sodium hydroxide to form hydrated calcium silicate (CSH) and hydrated aluminates after the dissolution of silica and alumina and combination with sodium hydroxide. This alkali-activated binder has a compressive strength similar to that obtained with Portland cement. So far, an important knowledge has been accumulating on the subject and several books [2-5] and reviews [6-9] have already been published on the subject. The common feature of all this research is the reaction between various raw materials and industrial wastes with alkalis-based reagents [10-26]. Depending on the

composition of precusors (i.e. aluminium, silicium and calcium contents) and those of activators (alkali oxydes or alkali hydroxydes and/or silicates) different chemistry and mechanisms occurs [27]. The precursor (solid phase) react with the alkaline salt (solid or dissolved) to form structures with differetns degree of crystallinity (i.e. zeolitic network, inorganic polymer or characterictic chains of calcium silicate hydrates). Despite the growing interest in alkali-activated binders, very little research has focused on the alkaline activation of precursor with very high calcium content (higher than in portland based cement) availiable for reaction and particularly as calcium carbonates. The main studies about alkaline activated binders with calcium carbonate (i.e limestone) were related to mixtures containing active silicate compounds as precursor [28, 29] or as activator [30]. The presence of limestone in these binders modify the molecular structure of the reaction products and enhance the stability underwater [29]. It leads to formation of cristalline carbonate phases such as pirssonite ($Na_2Ca(CO_3)_2.2H_2O$), gaylussite ($Na_2Ca(CO_3)_2.5H_2O$), portlandite ($Ca(OH)_2$) or thermonatrite (Na_2CO_3, H_2O) finely intermixed with amorphous calcium silicate hydrates (CSH), silica gel or calcium silicate gels (CSH), calcium-silicate gels incorporating sodium (NCSH), silica gels, sodium silicate gels (NSH), respectively. Depending on formulation parameters, these binders present a wide range of mechnical strength from 2 MPa to 32 MPa at 28 days with setting during conservation at 60°C for 24h followed by hardening at 20°C and relative humidity of 80-90% or hardening at 40°C, respectively. According to the same studies, the presence of cristalline phases in these binders could have differents effects on the matrix. They could cause a reduction in porosity, improving the compressive strength, but as they occupy a larger volume than the original hydroxides, they could generate internal stresses and loss of mechanical strength in the presence of moisture. The use of limestone as precusor and a solution of sodium hydroxide as activator without the addition of active silicate phases has only been investigated by one innovation patent filed in 2006 [31] and previous work carried out in our laboratory [32]. This study, firstly, focuses on the optimization of workability and mechanical strengths of mortar made with limestone filler and non reactive siliceous sand activated by a concentrate solution of sodium hydroxyde, secondly, in the identification of the reaction products and their microstructure using XRD, FTIR and SEM-EDX analyses and, finally, in the reliable quantification of the reaction products by a methodology based on thermal gravimetric analysis. This study is a first step for undestanding and manage the reactional process with the aim to

apply in the stabilisation and valorisation on wastes with high calcium carbonate content as wastes from food-processing industry (eggshells, crustacean shells) or from marble or cutstone and decorative stone quarries.

2. Materials

2.1. Limestone filler

The limestone used as a precursor in this study was a filler BETOCARB P2-MX supplied by OMYA France, commonly used as a mineral additive in concrete. Table 1 summarizes the main physical and chemical characteristics of the limestone filler.

Physical properties		Chemical composition	
Absolute density ($kg.m^{-3}$)	2600	$CaCO_3$ (%)	98.4
Blaine specific surface area ($m^2.g^{-1}$)	755	SiO_2 (%)	0.2
Fine particles < 63 µm (%)	96.1	Na_2O (%)	0.009
Activity index i28	0.80	S (%)	0.041

Table 1. Physical and chemical properties of limestone filler BETOCARB P2-MX.

Calcite ($CaCO_3$ 98.4%) was the only crystalline mineral identified by XRD (JCPDS 05-0586). The granulometry (determined by the supplier with a Metasizer 2000 laser particle sizer from Malvern Instruments) shows that 96% of the particles were smaller than 63 µm. Figure 1 shows their typical morphology.

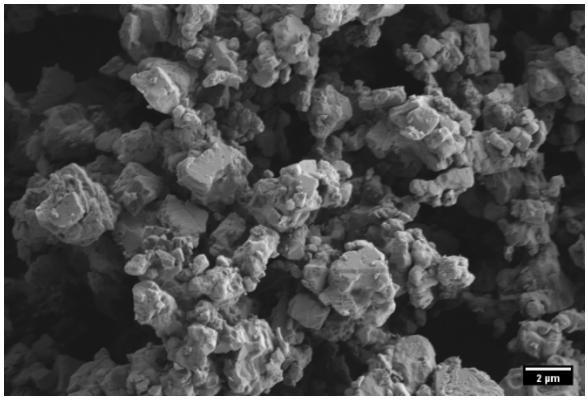

Figure 1–Morphology of limestone particles.

2. 2 Sand

Standardized sand in accordance with NF EN 196-1 [33] and ISO 679 [34] and corresponding to ASTM C778 [35], purchased from the SNL company (Leucate, France) was used for preparation of the mortars. Its composition was mainly siliceous (SiO_2 96.2%). Identification by XRD revealed a mineralogical composition based on well crystallized quartz (JCPDS 46-1045), which is considered to

be very weakly reactive with sodium hydroxide at room temperature. Particles are round shaped and their size distribution is regular between 0 and 2 mm (characteristics given by the supplier).

2. 3 Alkaline activator

The activator used in this study was a solution of sodium hydroxide (NaOH) at 12 and 13 mol/L obtained by the dilution of 50 $\%_{wt}$ concentrated soda solution in water, with a density of 1.515, from the Honeywell company. The pH of the activator solution was mesured with a pH-meter (Hanna Instrument HI 2221) equiped with a specific electrode for alkaline solutions and was around 15.

3. Mortar mixing, placing and curing

Before mixing, all materials were held in a climatic chamber at 20°C for at least 24 hours. Mortars were made of one part of limestone and three parts of sand (S/L =3), by mass, as in french standard cementitious mortars [33]. With the aim to obtain acceptable workability fot the mixtures and satisfactory compressive strength a preliminary series of mortars was prepared with varying alkaline-solution to limestone ratio (AS/L) between 0.52 and 0.68 mL/g and two moralities of soda solution of 12 and 13 mol/L. In these conditions, the water to binder ratio (W/B) was varying between 0.42 to 0.52 (Table 2). W was the mass of water (including water from the soda solution) and B was the mass of limestone and mass of sodium oxide (from the soda solution).

[NaOH] (mol/L)	AS/L (mL/g)	S/L	W/B ratio
12	0.52	3	0.42
12	0.60	3	0.47
12	0.68	3	0.52
13	0.60	3	0.46

Table 2. Parameters of preliminary mortars.

This optimization phase made possible to select a mortar with interesting results for fruther characterization in order to evaluate reactivity and quantify reaction products.

The mortars were mixed according to standard NF EN 196-1 [33], close to ASTM C305 [36] and three 40x40x160 mm prismatic specimens were cast in two layers, vibrated for 30 seconds each to release residual air bubbles. To minimize water evaporation at early ages, the molds were sealed in plastic bags. After 3 days the specimens were demolded. They were then cured for 11 days sealed in plastic bags at 20°C and then dried at 45°C for 14 days with the aim of eliminating free water in the mortar. Free water could be responsible of partial dissolution of reaction products [37] or internal stresses [30]. In our case, the elimination of free water of the mortar improves the mechanical strength [32].

4. Tests methods

The mortars have been characterized in different ways. For the optimization phase, the workability and mechanical strengths were measured according the methods given below. On the composition judged to be the most efficient (optimized), more tests were carried out: weight loss (during drying), porosity (at 32 days), thermal analysis (DTA-TGA at 32 days), FTIR (at 35 days), XRD (at 40 days), and SEM-EDX (at 52 days) according to the following methods.

4.1 Workability

The workability of fresh mortars was characterized according to NF P 18-452 [38], the processing method is similar to ASTM C 230 [39], French standard using a workability meter. The device is composed of a prismatic receiver that is divided into two parts, separated by a removable entity, and this prismatic receiver is put under vibration using an electric vibrator. The mortar is casted in one of the prismatic cavities in 4 successive layers in less than 2 minutes and 30 seconds. Each layer is tamped six times with a metal rod. The workability meter is put in vibration by taking off the removable entity that was used to retain the mortar. The mortar can flow freely under the action of the vibration, and the time (in seconds) is measured from the beginning of the flow until the mortar reaches a defined height on the second prismatic cavity.

4.2 Weight loss

The weight loss of the specimens, expressed as a percentage of the initial mass, was monitored throughout the curing time (28 days) by weighing once a day. This made it possible to check that the mass of the specimens had stabilized at the end of drying, before the following tests were made.

4.3. Mechanical strengths

The flexural and compressive strengths of the cured specimens were measured at 28 days according to standard NF EN 196-1 [33], close to ASTM C348 [40] and C349 [41], using 3R Quantech apparatus with loading speeds of 50 and 2400 N/s for flexural and compressive strength tests, respectively. The resulting flexural and compressive strength values were the means of three and six individual values, respectively.

4.4 Porosity

Porosity measurements in accordance with standards EN NF 1936 [42] and NF P18-459 [43] (processing method similar to ASTM C830 [44]) were made on representative samples after the

mechanical tests, using absolute ethanol instead of water in order to avoid the possible dissolution of alkali-activation products. Porosity (P) was calculated from equation (1) and the dry density of mortars (d) from equation (2).

$$P = 100\left[(m_{sat} - m_{dry})/(m_{sat} - m_{Eth)}\right] \quad (1)$$

$$d = \mathrm{d_{Eth}}\left[m_{dry}/(m_{sat} - m_{Eth})\right] \quad (2)$$

where m_{dry} was the dry mass of the samples at the end of curing, m_{sat}: the mass in air of ethanol-saturated surface-dry samples, m_{Eth}: the mass of ethanol-saturated samples and d_{Eth}: the density of ethanol.

4.5 FTIR

The FTIR spectra were recorded on ground samples (powders less than 0.315mm, sealed in plastics bags between grinding and testing) using an Alpha spectrometer with ATR cell (Bruker) in the range of 4000 to 600 cm^{-1}. Baseline correction, provided by the FTIR software, was applied to all spectra.

4.6. XRD

XRD analysis was carried out, on representative samples used for mechanical test, after grinding to of less than 0.315 mm powder and sealed in plastics bags until testing. The scans were run on an X-Pert 3 Powder instrument (Malvern Panalytical) with a copper anode ($\lambda_{(K\alpha)}$=1.540598 Å, with a step size of 0.0167° and a counting time of 0.5715 s/step from 2θ = 5° to 2θ = 70°.

4.7. Thermal analysis

Thermal analysis were carried out, on representative samples of the 3 prismatic specimens, used for mechanical test, after grinding to of less than 0.315 mm powder and sealed in plastics bags until testing. DTA-TGA tests were performed simultaneously with a STA 449 F1 Jupiter analyzer (Netzsch) from 25°C to 1000°C with a heating rate of 10°C/min under dynamic nitrogen atmosphere (50 mL/min). All the tests were performed using approximately 110 mg of powder. The results enabled us to identify and quantify the products formed in the mortar.

4.8. SEM-EDX

The microstructure of mortars was examined by scanning electron microscopy (SEM) on platinum-coated fractured pieces of cured specimen using a Gemini 300 (ZEISS) scanning electron microscope equipped with the Quantax 10 (Bruker) X-ray microanalysis detector. A working distance of 8.7 mm

was fixed and two acceleration voltages of 10 kV for surface imaging and 15 kV for elementary analysis were applied.

5. Results and discussion

5.1 Influence of composition parameters on workability and mechanical strength

Figure 2 presents the mechanical strength and workability as a function of the alkaline-solution to limestone ratio (AS/L) of mortars made with 12 mol/L alkaline solution.

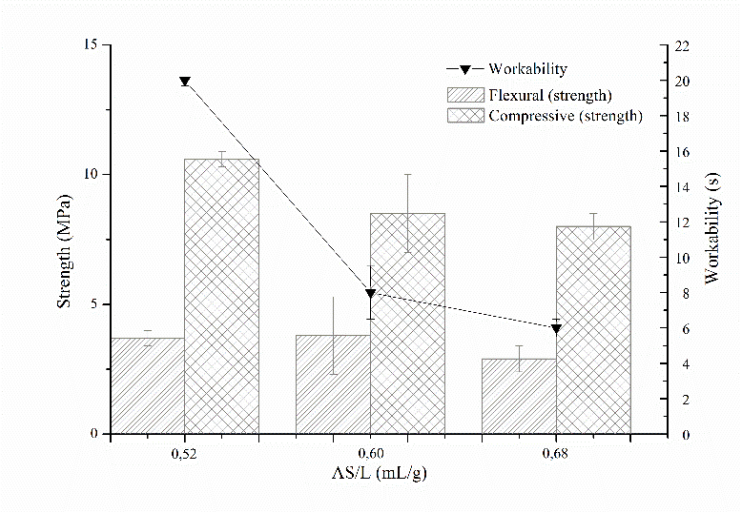

Figure 2–Mechanical strength and workability of mortars obtained with a sodium hydroxide solution at 12 mol/L.

The highest compressive strength was obtained for the smallest AS/L ratio (0.52 mL/g) and was around 10 MPa but, on the other hand, this mortar reached the limit of acceptable workability to ensure the homogeneity of the mortar under vibration (two times 30 seconds). The increase of the AS/L ratio, from 0.52 to 0.68, affects slightly the flexural strength of mortar, however, the compressive strength decreases of around 25% while the workability of the fresh mortar increases. These variations can be explained by the increase of the water relative amount (Table 2) in the mortar with the AS/L ratio which leads to a better wettability of particules but, as in cementitious materials, to an increase of porosity and a decrese of mechanical strength. The increase of the water amount seems to have greater influence than the proportional increase of the sodium hydroxide relative amount. Mortars with AS/L ratio higher than 0.68 mL/g with high workability have not sufficient compressive strength for applications in the field of construction.

With the aim to improve the mechanical strength of mortar maintaining the workability in acceptable values, the AS/L ratio of 0.60 mL/g was chosen for determine the influence of sodium hydroxide molarity on the properties of the mortar. Figure 3 presents the comparison of workability and mechanical strengths of mortars with the same AS/L ratio and varying sodium hydroxide molarity.

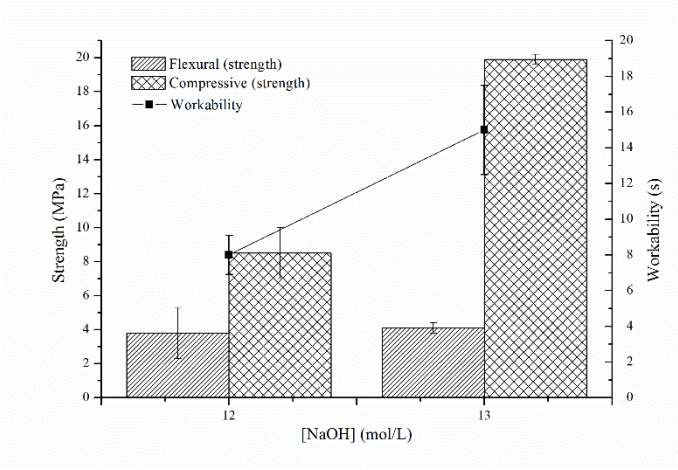

Figure 3–Mechanical strength and workability of mortars obtained with 12 and 13 mol/L sodium hydroxide solution and AS/L ratio of 0.60 mL/g.

It can be observed that the increase of 1 mol/L of NaOH in the solution more than doubles the compressive strength of the mortar, which reaches almost 20 MPa, when the water amount in the mortar remains constant. However, the flexural strength is not significantly affected by the variation of concentration of sodium hydroxide solution. Furthermore, the workability decreases and reaches almost that of the mortar with AS/L ratio equal to 0.52 ml/g (figure 2). Same behaviour, in terms of workability, was observed on alkali-activated natural pozzolan and limestone powder mortars made with sodium hydroxide solution above 10 to 14 M. It was attributed to the low water content in theses solutions that is not enough to wet all the particules [45].

The optimized formulation in terms of compressive strength with AS/L ratio equal to 0.60 mL/g and molarity equal to 13 M has been further studied. Its initial composition is presented in Table 3

	Relative amount ($\%_{wt}$)
SiO_2 (from sand)	60.08
$CaCO_3$ (from limestone)	20.47
Impurities (from sand and limestone)	2.73
Na_2O (from NaOH solution)	5.04
Free water	10.22
Bound water in NaOH	1.46
Total water	11.68
Total	100.00

198 Table 3–Composition of the optimized formulation of mortar.

199 5.2 Weight loss

200 Figure 4 shows the weight loss kinetics of the optimized mortar from demolding through to the end of
201 drying.

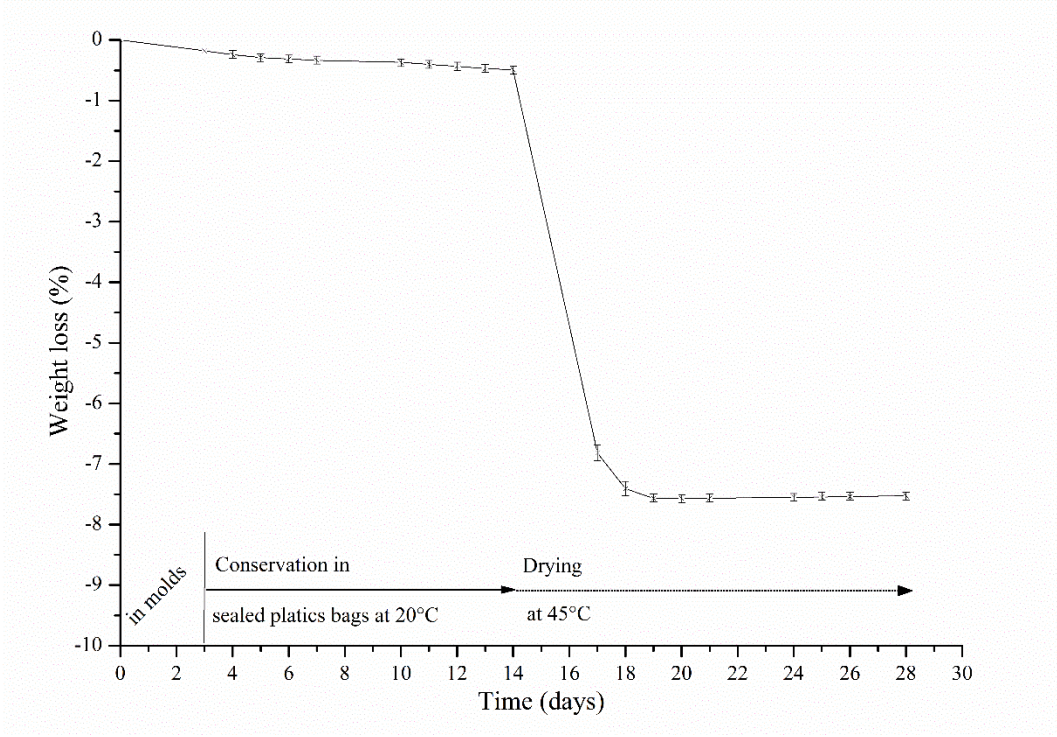

202

203 Figure 4–Weight loss of optimized formulation of mortar during 28 days curing.

204 For all specimens, a slight loss of weight (less than 0.5% of the initial mass) was observed during
205 storage in sealed bags at 20°C for 14 days. It was followed by a great loss of weight during the first
206 days of drying at 45°C. For all specimens the weight loss at the end of curing was around 7.5%. The
207 standard deviation for weight loss between the different specimens during 28 days curing was very
208 low (< 0.3%). This result indicates the great homogeneity of the mortar. As will be discussed below,
209 the amount of water removed by drying is significantly lower than the free water introduced into the
210 mortar's composition (10.22%, Table 3).

211 5.3 Identification of reaction products

212 Figure 5 shows the XRD pattern for the optimized alkali-activated mortar. Only the three or four most
213 important peaks for each identified crystalline phase have been referenced.

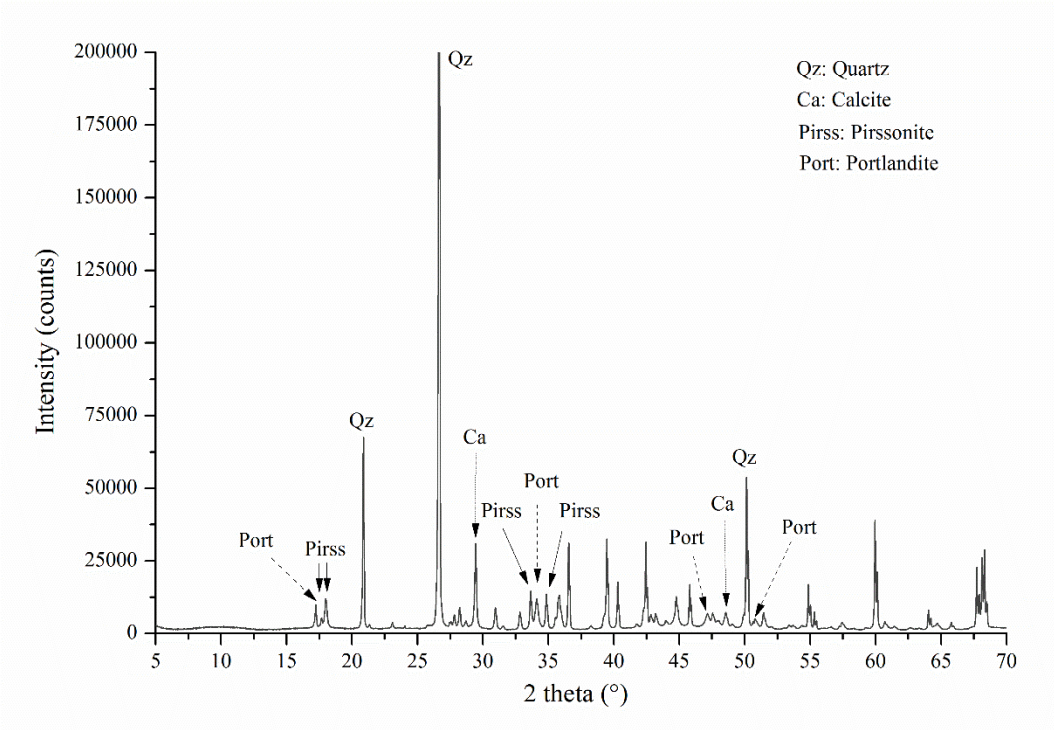

Figure 5–XRD pattern of optimized mortar after curing.

The crystalline phases present in the mortars resulting from alkali-activation of the limestone were pirssonite ($Na_2Ca(CO_3)_2.2H_2O$, JCPDS 24-1065) and portlandite ($Ca(OH)_2$, JCPDS 44-1481). There was also quartz (SiO_2, JCPDS 46-1045) from sand and a small amount of calcite ($CaCO_3$, JCPSD 05-0586), essentially from the unreacted limestone. This first result showed that most of the limestone reacted with sodium hydroxide to form a calcium/sodium carbonate hydrate and portlandite after curing, according to the chemical reaction (equation 3) [32, 37]:

$$2NaOH + 2CaCO_3 + 2H_2O \rightarrow Na_2Ca(CO_3)_2.2H_2O + Ca(OH)_2 \quad (3)$$

Figure 6 shows the FTIR spectra of initial materials (i.e. sand and limestone) in comparison with the spectra of alkali-activated limestone in mortar and in paste, prepared in the same conditions than the optimized mortar but without siliceous sand. The characteristic bands for siliceous sand and limestone were 1164, 1091, 1058, 796, 778, 694 cm^{-1} and 1795, 1396, 873, 713 cm^{-1}, respectively. The spectra of the paste and mortar samples present a split into two bands (1410 and 1480 cm^{-1}) of the limestone strongest peak (1396 cm^{-1}). Furthermore, six new peaks, at 3645, 3060, 1067, 903, 835 and 655 cm^{-1}, appears in the paste after alkali-activation and drying. Smallest characteristic peaks of limestone (1795, 875 and 711cm^{-1}) were also present in the alkali-activated paste. The FTIR spectrum of the mortar present the same peaks as the spectrum of the paste in addition to the characteristic peaks of

sand. Only the peak at 903 cm^{-1} was no longer visible due to the presence of sand. The changes observed for paste and mortar spectra (split and new peaks) are the result of reaction of the limestone with soda solution and could be attributed to formation of pirssonite and portlandite, as explicited behind.

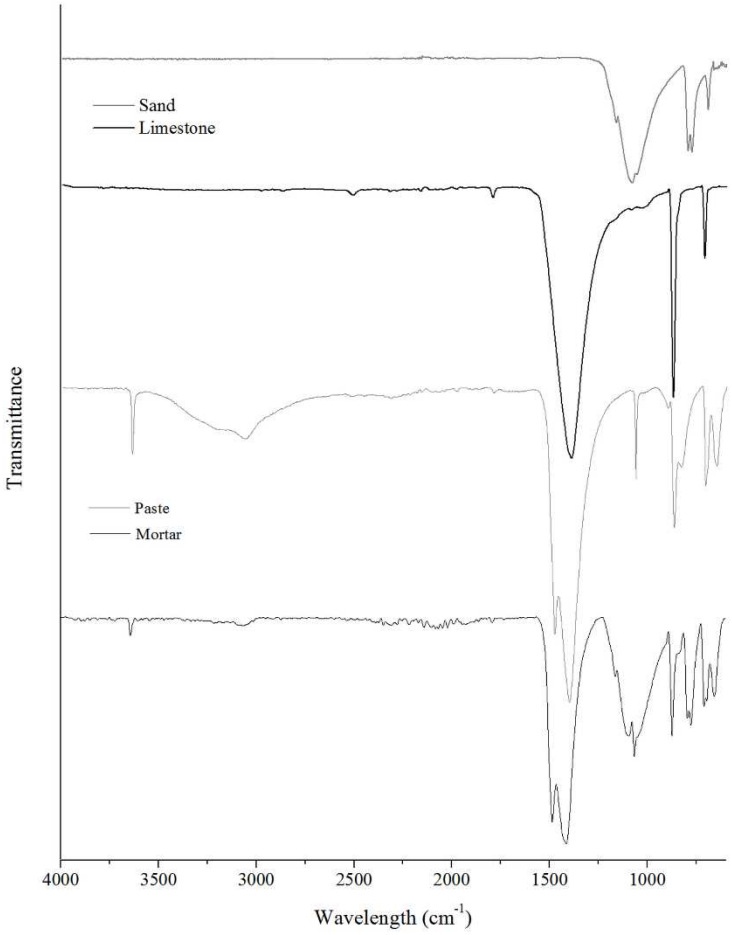

Figure 6–FTIR spectra of initial materials and alkali-activated limestone in paste and mortar.

FTIR studies have been performed on natural hydrated double carbonates [46-49] for years, and Table 4 shows their FTIR spectroscopic data. All the authors reported two vibration modes (υ_1 and υ_3) of the carbonate ion group in the natural pirssonite, even if it did not come from the same region of the world. They found that υ_3 divided into two bands, but were able to find three by peak deconvolution/analysis [49]. The other vibration modes (υ_2 and υ_4) show a single and a double band, respectively [46, 48], but Frost and Dickfos [49] reported a single band for υ_4. The wave numbers of the vibrations modes of the carbonate ion group differ slightly according to authors, but not the υ_1

mode, which is located at around 1067 cm^{-1}. Pirssonite also contains water molecules, which show two vibration modes υ_1 and υ_3 between 2900 and 3400 cm^{-1} [48, 49].

	Frequencies (cm^{-1})			
Assignment	Adler (1963)	Estep (1970)	Böttcher (1996)	Frost (2007)
		3430		3326 (OH unit)
υ_3 (H_2O)		3210	3214	3188 (OH unit)
υ_1 (H_2O)		3080	3074	3058 (OH unit)
				2954 (OH unit)
$\upsilon_1 + \upsilon_3$ CO_3^{2-}			2523	
$\upsilon_1 + \upsilon_3$ CO_3^{2-}			2459	
$\upsilon_1 + \upsilon_4$ CO_3^{2-}			1784	
$\upsilon_1 + \upsilon_4$ CO_3^{2-}			1733	
υ_2 H_2O			1697	
υ_3 CO_3^{2-}	1488	1481	1489	1480
υ_3 CO_3^{2-}				1465
υ_3 CO_3^{2-}	1414	1408	1423	1402
		1103		
υ_1 CO_3^{2-}	1068	1064	1069	
H_2O or υ_2 $^{12}CO_3^{2-}$		897	901	
υ_2 $^{12}CO_3^{2-}$	870	865	869	879
υ_2 $^{12}CO_3^{2-}$		830	834	
υ_4 CO_3^{2-}	712 and 699	705 and 700	709 and 700	704
υ_4 CO_3^{2-}		650	659	650

Table 4–FTIR spectroscopic data of pirssonite from Adler and al. [46], Estep and al. [47], Böttcher and al. [48], Frost and al. [49].

Our alkali-activated samples (paste and mortar) show almost all the characteristic vibration modes for pirssonite, as well for water molecules (3060 cm^{-1}) and for carbonate ion groups (υ_3 at 1480 and 1410 cm^{-1}, υ_1 at 1067 cm^{-1}, υ_2 at 835 cm^{-1}, υ_4 at 710 and 655 cm^{-1}) with some slight shifts compared to the bibliographic data. This can be explained by the possible deformation of carbonate units in the structure of our synthetic pirssonite. Furthermore, in our samples the bands at 875 and 711 cm^{-1} could be linked to the pirssonite and/or to the limestone contribution. The peak at 3645 cm^{-1} was attributed to the main band for portlandite [50] and was more or less visible in the alkali-activated samples. Other characteristic bands [50] were in the same region as pirssonite or limestone bands, so it has not been possible to identify them clearly.

The FTIR results confirm the XRD results and show that the identification of pirssonite is possible in a mortar because the additional peaks due to sand contribution do not mask the main characteristic peaks of pirssonite.

5.4 Microstructure of optimized mortar

Figure 7 shows the microstructure of the alkali-activated mortar at different scales.

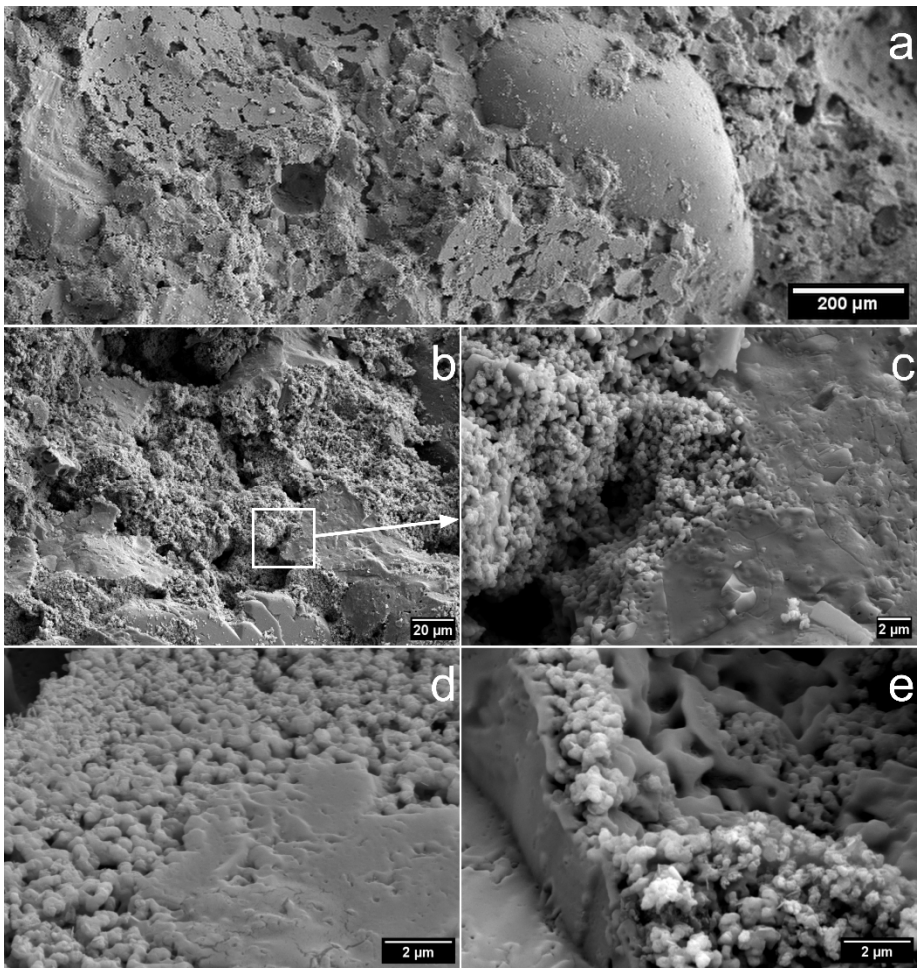

Figure 7–SEM images of alkali-activated mortar paste at different scales: (a) large field, (b) and (c) intermediate fields, (d) and (e) low field.

Figure 7a shows the different constituents of the mortar: the alkali-activated paste and its porosity as well as a round shaped grains of sand. The sand grain has a clean/smooth surface, without presence of silicate gels, which means that the sodium hydroxide solution did not attack their silica. This conclusion will be reinforced, thereafter, by the quantification of reaction products and consumption of reactants (§5.5), particularly, the total consumption of sodium hydroxide. In the paste, two types of microstructures were observed: one considered to be dense and one granular (grainy) (Figure 7b and 7c). The distribution of phases seems to be random, but grainy areas were often on the periphery of

dense zones, creating an intermediate or transition zone between the two types of microstructure where the grains become more and more joined (Figure 7d), as their coalescence leads to the formation of a dense zone. Both structures are three-dimensional as shown in Figure 7e. Porosity was also visible in all images: this comprised large pores of size between 50 and 10 µm and fine pores of less than 0.1 µm into the granular structures according to the spacing of the particles. This could explain the measured porosity on the optimized mortar: 20.09 ± 0.28% with a density of 1984 ± 24 kg/m^3.

Furthermore, a point-counting procedure, with EDX analyses, was made, in ten different areas in the paste, on these two different microstructures to identify them. Such procedure, using SEM or SEM-EDX analyses, has already been used to estimate the degree of hydration in cement pastes [51, 52] or for chracaterization of building derived materials [53] with good reliability. Figure 8 gathers together an example of results obtained in one of the ten paste areas analyzed.

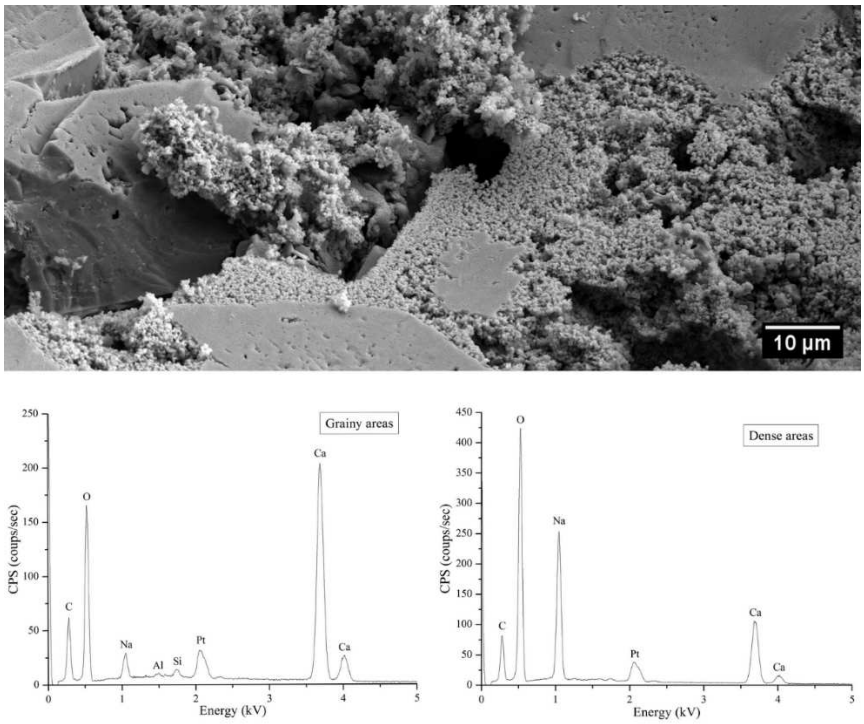

Figure 8–SEM image of dense and grainy areas in the paste and their respective EDX analyzes.

The same elements: C, O, Na, Ca were detected in both types of microstructures, but in different proportions. Al and Si were observed only in the granular zones. These were related to sand. Element quantification in the two different microstructures, in atomic percentages for sodium and calcium was obtained by the standardless PB-ZAF method, using EDX software. The Na/Ca ratio was calculated to assign microstructure to the reaction product. The dense and the granular microstructures had Na/Ca

ratios of 1.1 ± 0.1 and 0.1 ± 0.0, respectively. Theoretically, the Na/Ca ratios for pirssonite and portlandite or calcite are respectively 1.15 and 0.00. Thus, the compact microstructure was related to the pirssonite previously identified by XRD and FTIR experiments. The granular microstructure could be related to portlandite or calcite, but the shape and the size of this microstructure was closer to that of calcite in limestone (figure 1). No typical hexagonal plates of portlandite were observed. These observations confirm that the dissolution of filler grains by sodium hydroxide progressively leads to the crystallization of dense reaction products that explain the binding capacity of the mixture and the development of mechanical strength.

5.5 Quantification of the reaction products

Figure 9 shows the thermal analysis curves for standardized sand and the average thermal analysis curves for three samples of the three specimen of optimized mortar, after curing. For sand, no weight loss was observed and only one endothermic peak, at 568°C, associated with the allotropic transformation of quartz α into quartz β, was observed. For mortar samples, the following dissociation reactions were identified:

- Dehydration of pirssonite at 175°C (equation 4)

$$Na_2Ca(CO_3)_2.2H_2O \rightarrow Na_2Ca(CO_3)_2 + 2H_2O \quad (4)$$

- Dehydration of portlandite at 435°C (equation 5)

$$Ca(OH)_2 \rightarrow CaO + H_2O \quad (5)$$

- Decarbonatation of nyerereite at around 775°C (equation 6)

$$Na_2Ca(CO_3)_2 \rightarrow Na_2CO_3 + CaO + CO_2 \quad (6)$$

- Decarbonatation of the calcite of the unreacted limestone above 800°C (equation 7)

$$CaCO_3 \rightarrow CaO + CO_2 \quad (7)$$

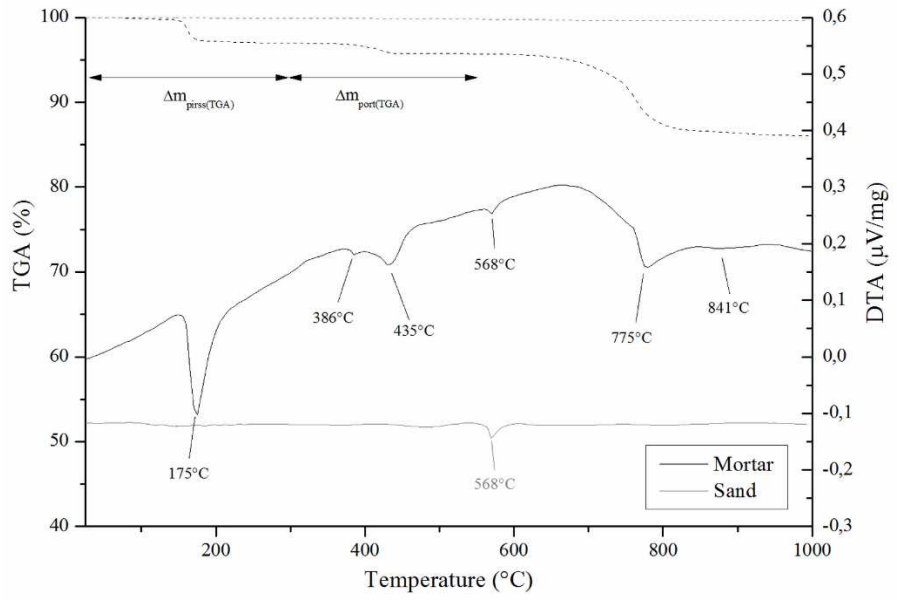

313

314 Figure 9–TGA and DTA curves of standardized sand and average curve of mortar samples after 28
315 days curing (dash: TGA and solid: DTA).

316 The dissociation temperatures of pirssonite and nyerereite were consistent with the literature [54]. The
317 thermal analysis curves also presented two crystallographic transformations without any variation in
318 mass. The first, around 386°C, corresponded to the transition from the low temperature form of
319 nyerereite to the high temperature form [55]. The second, around 568°C, related to sand contribution.
320 These results confirmed those obtained by XRD and FTIR showing that no additional amorphous
321 phase was present. The weight losses related to the dehydration of pirssonite and portlandite in dried
322 specimens, denoted $\Delta m_{pirss\ (TGA)}$ and $\Delta m_{port\ (TGA)}$ respectively, were measured on TG curves between 25
323 and 335°C and between 335 and 560°C respectively (figure 9). As the sample's TG curves were not
324 affected by the presence of sand (i.e. no interference noted) and the successive dissociation easily
325 identified for this type of mortar, the measures on these curves could be considered reliable.
326 Consequently, the following assumptions were made in order to quantifying, reaction products and
327 remaining reagents:
328 a) The sand and the limestone contained impurities; the accurate quantities of SiO_2 and $CaCO_3$ were
329 therefore recalculated considering them.
330 b) Grinding of the samples for DTA-TGA testing did not change the composition of the mortars,
331 particularly as regards the amount of pirssonite. However, as will be discussed below, it was possible

that portlandite formed from the alkali-activation reaction was partially carbonated during curing, crushing and storage up to the DTA-TGA tests.

5.5.1 Balance of water and quantification of reaction products

Firstly, two types of water were distinguished in the hardened material: free or evaporable water ($m_{free\ w}$) and bound water ($m_{bound\ w}$) in pirssonite and in portlandite. Secondly, the following assumptions were made:

a) Even though storage of the molds and specimens in sealed bags for 14 days (after demolding) prevents water evaporation, a very low loss of weight was observed (< 0.5%, Figure 4). This loss of weight is due to the free water in mortars and must be taken in account.

b) Drying at 45°C for 14 days leads to total evaporation of the rest of the free water in mortars (figure 3). Thus the relative mass of free water in the mortar after alkali-activation (expressed as %) was determined from the equation 8.

$$\Delta m_{free\ w} = 100[(m_0 - m_{28d})/m_0] \quad (8)$$

where m_0 was the mass of the specimens after casting (0 day) and m_{28d} was the mass of the specimens at the end of drying (28 days).

c) Considering the consumption of NaOH by the reaction to be complete (the limiting reagent in the reaction (equation 3) is in this case the sodium hydroxide), the relative mass of bound water in mortars after alkali-activation expressed as a % of the initial mass of mortar ($m_{bound\ w}$,) came only from the bound water in the reaction products (i.e. pirssonite and portlandite) and can be determined from the following equation.

$$\Delta m_{bound\ w} = \Delta m_{pirss\ w} + \Delta m_{portl\ w} \quad (9)$$

where $\Delta m_{pirss\ w}$ and $\Delta m_{portl\ w}$ were the relative mass of bound water in pirssonite and portlandite, respectively, calculated from the equations 10 and 11.

$$\Delta m_{pirss\ w} = \Delta m_{pirss\ (TGA)}\left[(100 - \Delta m_{free\ w})/100\right] \quad (10)$$

$$\Delta m_{portl\ w} = \Delta m_{portl\ (TGA)}\left[(100 - \Delta m_{free\ w})/100\right] \quad (11)$$

The total amount of water (Δm_{water}) in relation to the initial mass of mortar was calculated using equation (12):

$$\Delta m_{water} = \Delta m_{bound\ w} + \Delta m_{free\ w} \quad (12)$$

The water balance, corresponding to the difference between the initial amount of free and bound water in mixing with NaOH and the amount of water calculated from loss of weight and TGA (Δm_{water}, equation (12)) was also calculated. Table 5 shows the analytical results for all the previously determined quantities for each prismatic specimen tested.

Initial amount of water ($\%_{wt}$)	Measured amount of water ($\%_{wt}$)			Calculated amount of water ($\%_{wt}$)				Water balance ($\%_{wt}$)
	$\Delta m_{free\ w}$	$\Delta m_{pirss\ (TGA)}$	$\Delta m_{portl\ (TGA)}$	$\Delta m_{pirss\ w}$	$\Delta m_{portl\ w}$	$\Delta m_{bound\ w}$	Δm_{water}	
11.68 ± 0.00	7.53 ± 0.01	2.98 ± 0.08	1.25 ± 0.02	2.75 ± 0.08	1.16 ± 0.02	3.91 ± 0.07	11.44 ± 0.06	0.24 ± 0.06

Table 5–Initial, measured by experiments and calculated by equations (9) to (12) amounts of water for all specimens.

The three specimens had very close values for all the quantities of water determined, ensuring the homogeneity of the mortar. However, the calculated amount of water is slightly lower than the initial amount of water in the mixture (about 2% of the initial value). This water difference is probably due to incomplete reaction (equation 3) in the alkali-activation process. Sodium hydroxide, the limiting reagent for this reaction, should not have been completely consumed. In order to go further, an indirect approach to quantifying the remaining reagents is proposed in the following paragraph.

From the previous quantities of water determined by DTA-TGA, the relative amount of pirssonite and portlandite in the specimens in relation to the initial mass of the mortar (m_0) were determined according the following equations:

$$Pirss_{(TGA)} = \Delta m_{pirss\,w}\left(\mathrm{M_{pirss}}/2\mathrm{M_{water}}\right) \quad (13)$$

$$Portl_{(TGA)} = \Delta m_{portl\,w}\left(\mathrm{M_{portl}}/\mathrm{M_{water}}\right) \quad (14)$$

where M_{pirss}, M_{portl} and M_{water} were respectively the molar weights of pirssonite (242 g/mol), portlandite (74 g/mol) and water (18 g/mol).

On the other hand, it is also possible to determine the relative amount of portlandite (equation (15)) in the specimens indirectly, using the previous relative amount of pirssonite ($Pirss_{(TGA)}$) and the stoichiometric amount of both products from equation (3):

$$Portl_{(pirss)} = Pirss_{(TGA)}\left(\mathrm{M_{portl}}/\mathrm{M_{pirss}}\right) \quad (15)$$

383 This value does not take in account the possible carbonation of portlandite during curing and crushing
384 of the specimens, and must be compared with the previous value $\mathrm{Portl}_{(\mathrm{TGA})}$ determined directly from
385 DTA-TGA tests to evaluate the degree of carbonation of the portlandite.
386 The calculated amount of pirssonite ($Pirss_{(TGA)}$) was 18.50 ± 0.50 $\%_{wt}$. The portlandite quantities were
387 4.75 ± 0.08 $\%_{wt}$ and 5.66 ± 0.15 $\%_{wt}$ with direct DTA measurement ($Portl_{(TGA)}$) and undirect
388 measurement from pirssonite quantity ($Portl_{(pirss)}$), respectively. The three specimens had very close
389 values for all the quantities determined, ensuring that the mortar was homogeneous and the methods
390 employed reliable. The relative amount of portlandite determined directly by DTA-TGA tests ($Portl_{(TGA)}$)
391 was about 16 % lower than that determined indirectly by pirssonite (($Portl_{(pirss)}$). This confirmed
392 partial carbonation of the portlandite between the end of the activation reaction and the thermal
393 analysis experiments.
394 5.5.2 Quantification of remaining reagents
395 Based on the relative amount of pirssonite ($Pirss_{(\mathrm{TGA})}$), it is possible to determine the remaining
396 relative amounts of sodium oxide ($\Delta \mathrm{m}_{\mathrm{r}\,\mathrm{Na_2O}}$) from the remaining sodium hydroxide, and remaining
397 limestone ($\Delta \mathrm{m}_{\mathrm{r}\,\mathrm{CaCO_3}}$) according to equations 17 and 18.

398 $$\Delta m_{r\,Na_2O} = \Delta m_{Na_2O} - \left[Pirss_{(TGA)}\left(\mathrm{M_{Na_2O}}/\mathrm{M_{pirss}}\right)\right] \quad (17)$$

399 $$\Delta m_{r\,CaCO_3} = \Delta m_{CaCO_3} - \left[Pirss_{(TGA)}\left(2\mathrm{M_{CaCO_3}}/\mathrm{M_{pirss}}\right)\right] \quad (18)$$

400 where $\Delta \mathrm{m}_{\mathrm{Na_2O}}$ and $\Delta \mathrm{m}_{\mathrm{CaCO3}}$ were the initial relative quantities of solid sodium oxide (present in the
401 sodium hydroxide solution) and limestone used for preparation of the mortar (shown in Table 3),
402 $\mathrm{M}_{\mathrm{CaCO_3}}$ and $\mathrm{M}_{\mathrm{Na_2O}}$ were the molar weights of limestone (100 g/mol) and sodium oxide (62 g/mol),
403 respectively. Table 6 presents the composition of the mortar, taking into account the impurities from
404 sand and limestone, before and after the alkali reaction.

Mortar composition	Before alkali-activation ($\%_{wt}$) 0 day	After alkali-activation and before carbonation ($\%_{wt}$) 28 days
SiO_2 (from sand)	60.08	*60.08 ±0.00*
$CaCO_3$ (from limestone)	20.47	*5.18 ±0.41*
Impurities (from sand and limestone)	2.73	*2.73 ±0.00*
Pirssonite		*18.50 ±0.51*
Portlandite		*5.66 ±0.16*
Na_2O (from solution)	5.04	*0.23 ±0.13*

Free water	10.22	*7.53 ±0.01*
Bound water	1.46	*3.91 ±0.07*
Total water	11.68	*11.44 ±0.06*
Total	100.00	*99.90± 0.11*

Table 6– Composition before and after alkali-activation of each specimen of mortars.

The composition balance after alkali-activation was very close to 100%, confirming the consistency and reproducibility of the proposed methodology for determining free water, new products and remaining reagents. It will be seen that a very small amount (0.23%) of sodium oxide remains present in the mortar composition as sodium hydroxide solution after alkali-activation corresponding to lesser than 5% of its initial quantity. This confirms that the alkali-activation process was almost complete, consuming more than 95% of the initial amount of alkali activator. This sodium oxide remains as sodium hydroxide in the hardened mortar and includes 0.07% of bound water that must be considered when reducing the water balance (Table 5). On the other hand, the consumption of limestone was not complete; leaving about 25.3% of the initial amount unreacted, showing that the limiting reagent for the reaction is sodium hydroxide.

Finally, the alkaline reaction of limestone leads to the formation of a mortar composed of 18.50% pirssonite, 5.66% portlandite, 5.18% of remaining calcite, 0.23% of remaining sodium oxide, 2.73% impurities (from limestone and sand) and 60.08% silicon oxide, leaving 7.53% of evaporable water. Overall, we can consider that the binding capacity of the paste results from the pirssonite, portlandite and remaining calcite in a relative proportion of 3.5/1/1.

5.6 Comparison with published data in litterature

As seen above (section 5.1) the optimized mortar formulation present a flexural and compressive strenght of 4.1 ± 0.3 MPa and 19.9 ± 1.5 MPa, respectively. The compressive strength could be directly linked to pirssonite quantity if we take in account that the amount of pirssonite determined for one specimen (17.96 %) was lower than for the two others (18.59 and 18.69 %, respectively) and the compressive strength obtained for this specimen (17.5 and 16.2 MPa) was lower then that of the two others (21.6 MPa, 20.3MPa and 20.2 MPa, 19.9 MPa, respectively).

Comparatively to these value, the compressive strength observed by Ortega-Zavala [30] (less than 2 MPa obtained on mortars with W/B = 0,27 and setting at 60°C for 24h followed by a hardening at 20°C and a relative humidity of 80-90%), was significantly lower. This very low compressive strength

was explained by the presence of moisture which is responsible of internal stresses in alkali-activated limestone and therfore leads to a loss of mechanical strength. In the case of mortar with similar composition developped by Avila-Lopez [28], the compressive strength obtained depend on curing temperature: 2,44MPa after curing at 20°C (6% Na_2O, W/B = 0.3) and 19,10MPa after curing at 60°C (12% Na_2O, W/B = 0.5). The increase in Na_2O quantity and in the curing temperature leads to a higher compressive strength which is very close to that obtained on our optimized mortar. This result could be explained by the abscence of residual water when the mortars were cured at a temperaure upper than or equal to 45°C. Indeed, at 28 days the motars were totaly dryied (i.e. no moisture) and consequentely the internal stress could be eliminated.

As the main reaction products of the alkali-activate limestone are soluble in water like gypsum, the intended applications as building material must be considered only under indoor conditions. The elimination of free water by drying is necessary to obtain compressive strengh higher then that required for indoor building applications as plasters, screeds, partition walls, suspended ceilings (> 8 MPa).

The porosity and the density of the optimized mortar are 20.09 ± 0.28% and 1984 ± 24 kg/m^3, respectively. Unfortunately, theses parameters were not studied by others researchers who have studied the alkanie activation of limestone with sodium hydroxide but can be compared to traditional cement based and gypsum mortars. The density of the optimized alkali activated mortar is similar to traditional cement based mortars, 1990 kg/m^3 [56], and 12,5% higher than gypsum mortars, 1764 kg/m^3 [57] but it's porosity is 34% higher compared to traditional cement based mortars, 15% [56] and 38% lower compared to gypsum mortars, 28% [57].

The reduction of porosity in the alkali activated limestone mortar, certainly, must leed to an increase of mechanichal strengths and this may be considered by the reaction of remained unreacted limestone.

6. Conclusion

This study presents a new type of binder obtained by reaction between limestone and sodium hydroxide solution. The investigation on physical properties (strenght vs workability) of mortars, made with siliceous sand, on characterization of reaction products for optimized formulation (identification, microstructure and quantification) allows the following conclusions:

• Limestone can be used as a precursor to produce alkali activated binders after drying at 45°C.

460 • The compressive strength is in the range of 8 to 20 MPa, while the flexural strength was 3-4 MPa. It
461 depends on formulation parameters (water to binder ratio (W/B) or alkaline solution to limestone ratio
462 (AS/L) and sodium hydroxide molarity of the solution). An optimized mortar with a 13 M soda
463 solution and an W/B ratio equal to 0.46 (AS/L=0.60 mL/g) promotes the strength with an acceptable
464 workability.
465 • The proposed method, based on weight loss and thermogravimetric analysis, for quantification of
466 reaction products and remaining reagents have a high reliability and corroborate the balance of the
467 initial amounts but also the mechanical behaviour of the mortar.
468 • The matrix of the optimized mortar is a mix of crystalline sodium/calcium carbonate hydrate
469 (pirssonite), calcium hydroxide (portlandite) and unreacted limestone in a relative proportion of
470 3.5/1/1, without amorphous phase.
471 These results indicates that this new binder could be employed as an indoor construction material.
472 Further research is needed to improve knowledge of reaction mechanisms and the parameters that can
473 influence them and assess durability.
474 Acknowledgements
475 The X-ray diffraction tests were carried out in the Physics and Chemistry Forensics Division of
476 IRCGN (Institut de Recherche Criminelle de la Gendarmerie Nationale Française). Its staff is warmly
477 thanked.
478 The FTIR and the SEM-EDX analyses were carried out in Ermeece Laboratory (EA1391) and in the
479 ″Microscopies & Analyses″ imaging facility, Federation I-Mat (FR4122) of the CY Cergy Paris
480 Université (France), respectively.
481 Funding:
482 This research did not receive any specific grant from funding agencies in the public, commercial, or
483 not-for-profit sectors.
484 References
485 [1] AO. Purdon, The action of alkalis on blast furnace slag, J. Soc. Chem. Ind. 59 (1940) 191-202.
486 [2] J. Davidovits, Geopolymer. Chemistry and Applications, first ed., Institute Geopolymere, Saint-
487 Quentin, France, 2008.

[3] C. Shi, P.V. Krivenko, D. Roy, Alkali-activated cements and concretes, Taylor & Francis, Abingdon and New York, 2006.

[4] J.L. Provis, J.S.J. van Deventer, Geopolymers, structure, processing, properties and industrial applications, Woodhead Publishing Limited and CRC Press LLC, 2009.

[5] J.L. Provis, J.S.J. van Deventer, Alkali activated Materials. State of the art Report. RILEM TC 224-AAM, Springer, 2014.

[6] F. Pacheco-Torgal, J. Castro-Gomes, S. Jalali, Alkali-activated binders: A review Part 1. Historical background, terminology, reaction mechanisms and hydration products, Constr. Build. Mater. 22 (2008) 1305–1314. https://doi.org/10.1016/j.conbuildmat.2007.10.015

[7] A. Palomoa, P. Krivenkob, I. Garcia-Lodeiroa, E. Kavalerovab, O. Maltsevaa, A. Fernández-Jiménezа. A review on alkaline activation: new analytical perspectives, Mater. Construcc. 64 (2014), e022. https://doi.org/10.1016/j.conbuildmat.2007.10.015

[8] T. Luukkonen, Z. Abdollahnejad, J. Yliniemi, P. Kinnunen, M. Illikainen, One-part alkali-activated materials: A review, Cem. Concr. Res. 103 (2018) 21-34. https://doi.org/10.1016/j.cemconres.2017.10.001

[9] Z. Tang, W. Li, Y. Hu, J. L. Zhou, V. W.Y. Tam, Review on designs and properties of multifunctional alkali-activated materials (AAMs), Constr. Build. Mater. 200 (2019) 474-489. https://doi.org/10.1016/j.conbuildmat.2018.12.157

[10] H. Xu and J. S. J. van Deventer, Microstructural characterization of geopolymers synthesized from kaolinite/stilbite mixtures using XRD, MAS-NMR, SEM/EDX, TEM/EDX, and HREM, Cem. Concr. Res. 32 (2002) 1705-1716. https://doi.org/10.1016/S0008-8846(02)00859-1

[11] K. El Hafid, M. Hajjaji, H. El Hafid, Influence of NaOH concentration on microstructure and properties of cured alkali-activated calcined clay, J. Build. Eng. 11, (2017) 158-165. https://doi.org/10.1016/j.jobe.2017.04.012

[12] A. Fernández-Jiménez, M. Monzó, Vicent, A. Barbab, A. Palomoa, Alkaline activation of metakaolin fly ash mixtures: Obtain of Zeoceramics and Zeocements, Micropor. Mesopor. Mat. 108 (2008) 41-49. https://doi.org/10.1016/j.micromeso.2007.03.024

[13] A. Chaipanich, K. Wianglor, M. Piyaworapaiboon, S. Sinthupinyo, Thermogravimetric analysis and microstructure of alkali-activated metakaolin cement pastes, J. Therm. Anal. Calorim. 138 (2019) 1965–1970. https://doi.org/10.1007/s10973-019-08592-z

[14] R. Pouhet, M. Cyr, R. Bucher, Influence of the initial water content in flash calcined metakaolin-based geopolymer, Constr. Build. Mater. 201 (2019) 421-429. https://doi.org/10.1016/j.conbuildmat.2018.12.201

[15] N. R. Rakhimova, R. Z. Rakhimov, V. P. Morozov, A. R. Gaifullin, L. I. Potapova, A. M. Gubaidullina, Y. N. Osin, Marl-based geopolymers incorporated with limestone: A feasibility study, J. Non Cryst. Solids, 492 (2018) 1-10. https://doi.org/10.1016/j.jnoncrysol.2018.04.015

[16] S. A. Bernal, E. D. Rodriguez, R. Mejía de Gutiérez, J. L. Provis, Performance of alkali-activated slag mortars exposed to acids, J. Sustain. Cement-Based Mater. 1 (2012) 138-151. https://doi.org/10.1080/21650373.2012.747235

[17] P. S. Deb, P. Nath, P. K. Sarker, The effects of ground granulated blast-furnace slag blending with fly ash and activator content on the workability and strength properties of geopolymer concrete cured at ambient temperature, Material and Design 62 (2014) 32-39. https://doi.org/10.1016/j.matdes.2014.05.001

[18] B. V. Rangan, D. Hardjito, S. E. Wallah, D. M. J. Sumajouw, Properties and application of fly-ash-based concrete, Material Forum, volume 30, Edited by R. Wuhrer and M. Cortie, © Institute of materials Engineering Australasia Ltd, 170-175, 2006

[19] O. Burciaga-Díaz, J.I. Escalante-García, Structure, mechanisms of reaction, and strength of an alkali-activated blast-furnace slag", J. Am. Ceram. Soc. 96 (2013) 3939–3948. https://doi.org/10.1111/jace.12620

[20] R. Martinez-Lopez, J. I. Escalante-Garcia, Alkali activated composite binders of waste silica soda lime glass and blast furnace slag: Strength as a function of the composition, Constr. Build. Mater. 119 (2016) 119-129. https://doi.org/10.1016/j.conbuildmat.2016.05.064

[21] K. K. Ramagiri, A. Kar, Effect of high-temperature on the microstructure of alkali-activated Binder, Materials Today: Proceedings 28 (2020) 1123-1129. https://doi.org/10.1016/j.matpr.2020.01.093

[22] S. A. Bernal, J. L. Provis, B. Walkley, R. San Nicolas, J. D. Gehman, D. G. Brice, A. R. Kilcullen, P. Duxson, J. S. J. van Deventer, Gel nanostructure in alkali-activated binders based on slag and fly ash, and effects of accelerated carbonation, Cem. Concr. Res. 53 (2013) 127-144. https://doi.org/10.1016/j.cemconres.2013.06.007

[23] S. Ahmari, X. Ren, V. Toufigh, L. Zhang, Production of geopolymeric binder from blended waste concrete powder and fly ash, Constr. Build. Mater. 35 (2012) 718-729. https://doi.org/10.1016/j.conbuildmat.2012.04.044

[24] M. Cyr, R. Idira, T. Poinot, Properties of inorganic polymer (geopolymer) mortars made of glass cullet, J. Mater. Sci. 47 (2012) 2782-2797. https://doi.org/10.1007/s10853-011-6107-2

[25] R. Idira, M. Cyr, A. Pavoine, Investigations on the durability of alkali-activated recycled glass, Constr. Build. Mater. 236 (2020) 117-477. https://doi.org/10.1016/j.conbuildmat.2019.117477

[26] J. Payá, M. V. Borrachero, J. Monzó, L. Soriano, M. M. Tashima, A new geopolymeric binder from hydrated-carbonated cement, Mater. Lett. 74 (2012) 223-225. https://doi.org/10.1016/j.matlet.2012.01.132

[27] J. S. J. Van Deventer, J. L Provis, P. Duxson, D. G. Brice, Chemical research and climate change as drivers in the commercial adoption of alkali activated materials. Waste Biomass Valor, 1 (2010) 145-155. https://doi.org/10.1007/s12649-010-9015-9

[28] U. Avila-López, J. M. Almanza-Robles, J. I. Escalente-García, Investigation of novel waste glass and limestone binders using statistical methods, Constr. Build. Mater. 82 (2015) 296-303. https://doi.org/10.1016/j.conbuildmat.2015.02.085

[29] L. E. Menchaca-Ballinas, J. I. Escalente-García, Limestone as aggregate and precursor in binders of waste glass activated by CaO and NaOH, Constr. Build. Mater. 262 (2020) 120013. https://doi.org/10.1016/j.conbuildmat.2020.120013

[30] D. E. Ortega-Zavala, J. L. Santana-Carrillo, O. Burciaga-Díaz, J. I. Escalante-García, An initial study on alkali activated limestone binders, Cem. Concr. Res. 120 (2019) 267-278. https://doi.org/10.1016/j.cemconres.2019.04.002

[31] P. Pichat, Fabrication d'un matériau solide à partir d'un hydroxyde alcalin, *Patent* WO2006087484A3, August 2006.

571 [32] J-L. Gallias, A. Cousture, F. Forest, P. Pichat, Etude de l'activation alcaline du filler calcaire par
572 l'hydroxyde de sodium, NoMAD Conference, 7-8 novembre 2015, Douai, France.
573 [33] AFNOR (2006) NF EN 196-1 Methods of testing cement-part1: determination of strength.
574 [34] AFNOR (2009) ISO 679 Cement-Test methods-Determination of strength.
575 [35] ASTM (2017) C778 Standard specification for standard sand
576 [36] ASTM (2019) C305 Standard specification for mortar of unit masonry
577 [37] A. Cousture, N. Renault, P. Pichat, J-L. Gallias, Etude de l'activation alcaline de composés
578 calcaires et siliceux, NoMAD Conference, 7-8 novembre 2018, Liège, Belgique.
579 [38] AFNOR (2017) NF P 18-452 Concretes — Measuring the flow time of concretes and mortars
580 using a workabilitymeter
581 [39] ASTM (2021) C230 Standard specification for flow table for use in tests of hydraulic cement
582 [40] ASTM (2021) C348 Standard test method for flexural strength of hydraulic-cement mortars
583 [41] ASTM (2018] C349 Standard test method for compressive strength of hydraulic-cement mortars
584 (using portions of prisms broken in flexure)
585 [42] AFNOR (2007) NF EN 1936 Natural stone test methods: determination of real density and
586 apparent density, and of total and open porosity.
587 [43] AFNOR (2010) NF P18-459 Test for hardened concrete: Porosity and density test.
588 [44] ASTM (2016) C830 Standard test method for apparent porosity, liquid absorption, apparent
589 specific gravity, and bulk density of refractory shapes by vacuum pressure
590 [45] A. A. Adewumi, M. A. M. Ariffin, M. O. Yusuf, M. Maslehuddin, M. Ismail, Effect of sodium
591 hydroxide concentration on strength and microstructure of alkali-activated natural pozzolan and
592 limestone powder mortar, Constr. Build. Mater. 271 (2021) 121530.
593 https://doi.org/10.1016/j.conbuildmat.2020.121530
594 [46] H. H. Adler, P. F. Kerr, Infrared spectra, symmetry and structure relations of some carbonate
595 minerals, Amer. Mineral. 48 (1963) 839-853.
596 [47] P. A. Estep, J. J. Kovach, A. L. Hiser, C. Jr. Karr, Characterization of carbonate minerals from oil
597 shales and coals by infrared spectroscopy, Plenum Press, New York – London, 1970.

598 [48] M. E. Böttcher, P.-L. Gehlken, Dehydration of natural gaylussite ($Na_2Ca(CO_3)_2$, $5H_2O$) and
599 pirssonite ($Na_2Ca(CO_3)_2$, $2H_2O$) as illustrated by FTIR spectroscopy, N. Jb. Miner. Mh. 2 (1996) 73-
600 91.
601 [49] R. L. Frost, . M. Dickfos, Hydrated double carbonates – A Raman and infrared spectroscopic
602 study, Polyhedron, 26 (2007) 4503-4508. https://doi.org/10.1016/j.poly.2007.06.003
603 [50] B. Lafuente, R. T. Downs, H. Yang, N. Stone, The power of databases: the RRUFF project. In:
604 Highlights in Mineralogical Crystallography, T. Armbruster, R. M. Danisi (Eds.) Berlin, Germany, W.
605 De Gruyter, 2015, pp.1-30. Database accessible from: http://rruff.info/
606 [51] X. Feng, E. J. Garboczi, D. P. Bentz, P. E. Stutzman, T.O. Mason, Estimation of the degree of
607 hydration of blended cement pastes by a scannng electron microscope point-counting procedure, Cem.
608 Concr. Res. 34 (2004) 1787-1793. https://doi.org/10.1016/j.cemconres.2004.01.014
609 [52] Q. Hu, M. Aboustait, T. Kim, M. T. Ley, J. C. Hanan, J. Bullard, R. Winarski, V. Rose, Direct three-
610 dimensional observation of the microstructure and chemistry of C_3S hydration, Cem. Concr. Res. 88
611 (2016) 157-169. https://doi.org/10.1016/j.cemconres.2016.07.006
612 [53] A. K. Suluguru, M. Jayatheja, A. Kar, A. GuhaRay, S. R. Surana, N. James, Experimental studies on
613 the microstructural, physical and chemical characteristics of building derived materials to assess their
614 suitability in ground improvement, Constr. Build. Mater. 156 (2017) 921-932.
615 https://doi.org/10.1016/j.conbuildmat.2017.09.058
616 [54] R. M. Dheilly, J. Tudo, Contribution à l'étude de la Gaylussite, C. R. Acad. Sci. Paris, 325 (1997)
617 407-414.
618 [55] D.R. Johnson, W. A. Robb, Gaylussite: Thermal Properties by simultaneous thermal analysis,
619 Am. Mineral. 58 (1973) 778-784.
620 [56] Q. Zeng, K. Li, T. Fen-Chong, P. Dangala, Effect of porosity on thermal expansion coefficient of
621 cement pastes and mortars, Constr. Build. Mater. 28 (2012) 468-475.
622 https://doi.org/10.1016/j.conbuildmat.2011.09.010
623 [57] J. Krejsová, M. Doleželová, R. Pernicová, P. Svora, A. Vimmrová, The influence of different
624 aggregates on the behavior and properties of gypsum mortars, Cem. Concr. Compos. 92 (2018) 188-
625 197. https://doi.org/10.1016/j.cemconcomp.2018.06.007